International Journal of Modern Physics B
Vol. 25, No. 6 (2011) 885–896

DOI: 10.1142/S0217979211057980

World Scientific
www.worldscientific.com

CLAMPING LOSSES OF FOLDED- AND STRAIGHT-BEAM MEMS RESONATORS MADE FROM POLYCRYSTALLINE 3C-SiC FILMS

WEN-TENG CHANG

Department of Electrical Engineering, National University of Kaohsiung, No. 700, Kaohsiung University Road, Nan-Tzu District, Kaohsiung 811, Taiwan
wtchang@nuk.edu.tw

Received 4 February 2009

This paper presents an analysis of clamping losses in microelectromechanical systems (MEMS)-based, flexural mode silicon carbide (SiC) lateral resonators. The study includes folded- and straight-beam resonators made from (111) polycrystalline 3C-SiC side by side. The device testing was conducted at 30 μTorr using a transimpedance-amplifier-based circuit to measure the total quality factor. It was found that thermoelastic damping (TED) in SiC MEMS-based lateral resonators has minimal contributions to overall energy dissipation in the aforementioned devices. Moreover, the difference in material losses of these devices is negligible due to their similar microstructure. In this case, clamping losses are responsible when one is comparing the energy dissipation mechanism of these two types of resonators. The findings showed that the total losses for a folded-beam resonator were reduced by more than 10 times that for a straight-beam resonator when the beam lengths were set at 150 μm and operated at the same level of resonant frequency. The clamping coefficient of the folded-beam resonator was between 0.7 and 1.8, suggesting that the effective dimension of a folded-beam resonator should include part of the proof mass.

Keywords: Folded-beam resonator; straight-beam resonator; clamping loss; quality factor.

1. Introduction

Microelectromechanical systems (MEMS)-based resonators have attracted the attention of the radio frequency (RF) communications community, due to their high quality factors (Q's) and their potential for integration with Si integrated circuits (ICs).[1,2] These RF applications demand a technological device that can efficiently perform very low to ultrahigh frequencies, a range that can be achieved by MEMS and nanoelectromechanical systems (NEMS).[1–4] Consequently, silicon carbide (SiC) has become a promising material for RF MEMS due to its high Young's-modulus-to-density ratio relative to Si, thus increasing the acoustic velocity and fundamental resonant frequency of the vibrating structure relative to it. However, this is possible only with high quality factors.[5] Hence, a low quality factor will lead only to poor

resonators due to high energy dissipation. It should be noted, however, that the Young's-modulus-to-density ratio will result in higher resonant frequencies regardless of the quality factor. Surface micromachined, flexural mode resonators offer a convenient means of characterizing the properties of the materials — properties that influence the quality of performance, such as Q. Moreover, cubic SiC (3C-SiC) is the only polytype that can epitaxially grow on a silicon substrate, among the 250 polytypes of SiC. In view of this, this study was conducted to investigate the clamping mechanisms in cubic SiC resonators. The inverse of the quality factor (Q^{-1}) is a common and simple way of expressing energy loss in an oscillating system. In addition, the inverse quality factor is defined as the energy dissipated over the energy stored in a dynamic system over one oscillation cycle. Meanwhile, energy losses in a microscale resonator can be attributed to several factors, including gas damping, surface losses, thermoelastic damping (TED), internal friction of the structural material and clamping losses.[6,7] The total energy loss in the system is simply the sum of the energy loss components and can be written as follows:

$$Q_{\text{total}}^{-1} = Q_{\text{air}}^{-1} + Q_{\text{TED}}^{-1} + Q_{\text{material}}^{-1} + Q_{\text{clamping}}^{-1} + \cdots . \tag{1}$$

To obtain the specific factor of the energy loss mechanism, efforts should be made toward minimizing the impact of the others. The total energy loss of a resonator can be extracted directly from the measured frequency response of the device. The gas damping has been proven to be negligible under a low pressure for different geometries.[8–10] Surface losses are caused by the chemical reaction of the surface of a resonator, which is an important issue in nanoresonators but not in microresonators.[11,12] TED is in the form of heat released from the material. The heat is absorbed while the object is decompressed or in a tensile state. A thermal gradient is created as heat flows from high temperature to low temperature, resulting in the flow of heat. This flow depends on the thermal conductivity of the material. The process is irreversible, because the energy is dissipated during the event. Any device under cyclic motion, such as a micromechanical resonator, loses energy by TED, particularly through bending beams. This is the product of a temperature-dependent function and a frequency-dependent one.[13] The maximum Q_{TED}^{-1} of a resonator can thus be calculated from the known material properties with an assumption that the local temperature is known. The TED is mainly distributed at the supporting beams because of the higher strain gradient at these locations.[14] Although TED and material losses are difficult to distinguish because both of them are subject to material properties, material losses are dependent only on the grain size of the material. The energy of the material losses is dissipated at the grain boundaries by sliding. A smaller grain size results in a higher density of local sliding. This dissipation is attributed to the grain boundaries but not to the geometric design.[15–18] However, the clamping losses of resonators are dependent on their own design.[19] For a flexural mode, a two-dimensional resonator, such as a cantilever and a simple

doubly clamped microbridge, the clamping energy dissipation can be written as

$$Q^{-1}_{\text{clamping}} = \beta\left(\frac{w}{l}\right)^3, \tag{2}$$

where w and l are the width and length of the beam, respectively. The coefficient β depends on the design of the resonator, with a value of 0.46 for a cantilever vibrator and 1.1 for a doubly clamped microbridge resonator.[20,21] To the best of our knowledge, this β is applied only on a straight-beam resonator, but no one has ever determined this value because its structure and equivalent beam width and length are dependent on the design dimensions of the folded-beam resonators — specifically, the effective proof mass and beams. Folded-beam resonators are common flexural mode resonators, but their clamping losses compared with those of straight-beam resonators have not yet been evaluated. Although the resonators have several energy loss mechanisms, they can be isolated by a proper experimental design. By integrating such measurements with the analyses obtained from theories, there will be a better understanding of the components dominant in energy loss.

2. SiC Film Growth and Resonator Fabrication

A series of resonators was fabricated from poly-SiC deposited by LPCVD. In this case, the substrates consisted of Si wafers capped with a thermally grown 1.5-micron-thick SiO_2 film. The poly-SiC films were initially deposited directly on top of the oxide surface using dichlorosilane (DCS) and acetylene as precursors. Under these conditions, residual film stress was reported as tensile residue stress of 44 MPa, and the resistivity of the films was measured to be 3 Ωcm.[22]

The poly-SiC resonators made from the unmodified LPCVD films were originally developed for a previous study,[21] and in the current work they are denoted as type D. Additionally, these type D resonators use poly-SiC as the structural material, SiO_2 as the sacrificial layer, and (100) Si as the substrate. As a result of these devices that make up type D, two resonator designs were fabricated side by side: a folded-beam resonator, named type D_f [Fig. 1(a)], and a straight-beam resonator, named type D_c [Fig. 1(b)]. Type D_c has a spontaneously higher spring constant as compared to type D_f in terms of clamping design. Type D_c was designed with

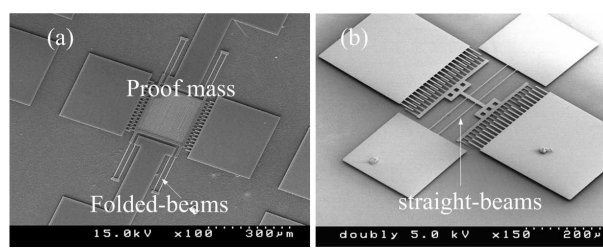

Fig. 1. Plan-view SEM micrograph of a folded-beam resonator (a) and a straight-beam resonator (b) fabricated from polycrystalline 3C-SiC, identified as type D_f and type D_c.

Table 1. Dimension of folded-beam and straight-beam resonators and the modeling resonant frequencies by ANSYS.

	Device	D_{f1} (folded-beam)	D_{c1} (straight-beam)
Dimensions	Beam width (m)	2.05×10^{-6}	1.50×10^{-6}
	Beam length (m)	1.00×10^{-4}	1.50×10^{-4}
	Proof mass (m^2)	2.37×10^{-8}	1.51×10^{-8}
	Truss area (m^2)	6.93×10^{-10}	—
	Beam area (m^2)	1.64×10^{-9}	9.00×10^{-10}
	Density (kg/m^3)	3.21×10^{3}	3.21×10^{3}
Assumptions	Poission ratio	0.17	0.17
	Young's modulus (Pa)	3.80×10^{11}	3.80×10^{11}
Modeling	Resonant frequency (Hz)	45671	34460

interdigital comb fingers similar to type D_f, but type D_c was clamped on the two ends to have a larger coefficient β in Eq. (2). Table 1 shows the dimension of the folded-beam and straight-beam resonators. The ANSYS results verified the resonant frequencies using these parameters.

3. Resonators Measurement

3.1. *Experimental setup*

For the lateral resonators of the type described in this work, it is possible to observe a shuttle oscillating in the air when using a microscope with proper magnification. In this situation, a function generator can be used to actuate the resonators by simply tuning the output frequency of the generator to the natural frequency of the resonator. The setup does not require external amplification circuits, and therefore electrical connection can be made directly to the contact pads of the device using micromanipulators. The microscope on a standard probe station is of sufficient magnification to enable such testing. A wideband amplifier is usually required to magnify AC voltage, because the function generator has a maximum output voltage of only 10 V and is not capable of providing a voltage high enough to drive the shuttle at atmospheric pressure, which usually requires at least 20 V. The oscillation is of lateral mode, as shown in Fig. 2. The natural frequency of the resonator is twice the frequency displayed on the function generator, because the shuttle is attracted by both positive and negative voltages without bias.

The resonant frequency of the resonators can therefore be determined by optical observation prior to mounting on a printed circuit board (PCB). The PCB was used as the physical base and interconnecting layer on which the test circuit was constructed. The chip-based MEMS resonator and a Philips SA5211 transimpedance amplifier with a gain of 14 kΩ were mounted on the PCB, as shown in Fig. 3(a). While oscillating, the MEMS resonator generates a motional current converted to a voltage signal by the transimpedance amplifier. In this study, the Philips SA5211

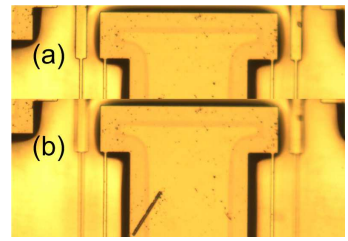

Fig. 2. Lateral oscillation of the resonator in this work: (a) static and (b) oscillating.

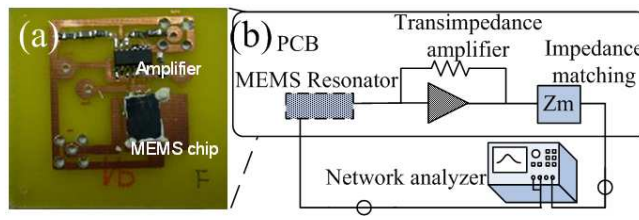

Fig. 3. Optical photograph of the PCB with electronics and MEMS resonator chip (a) and schematic of the measurement block diagram (b).

transimpedance amplifier was purposely chosen, as it uses a bipolar junction transistor (BJT) differential amplifier capable of providing a low noise output signal. In addition, its bandwidth reaches 180 MHz, which can meet the intended measurement range. A wedge bonder was likewise used to bond 25-micron-diameter Al wires to the device contact pads and the PCB. Figure 3(b) shows a schematic of the measurement block diagram. The gain of the PCB-based testing circuit was measured by an Agilent 4395A network/spectrum analyzer with optional impedance measurements that provide a working range from 10 Hz to 500 MHz with a minimum of 1 mHz resolution. The circuit was then put into a vacuum system which is equipped with a diffusion pump and is capable of reaching pressures even to the extent of about 1 μTorr. The testing of the device was conducted at 30 μTorr using a PCB-based transimpedance-amplifier-based circuit to facilitate the actuation and detection. The motional current from the MEMS resonator was also amplified by the transimpedance amplifier placed next to the MEMS chip. During the testing, the transmission spectrum (S_{21}) determined the total quality factor of the circuit containing the MEMS resonator.

3.2. *Experimental results*

The quality factor was calculated using the 3 dB bandwidth divided by the resonant frequency:

$$Q = \frac{f_r}{\Delta f_{3\,\mathrm{dB}}}\,. \tag{3}$$

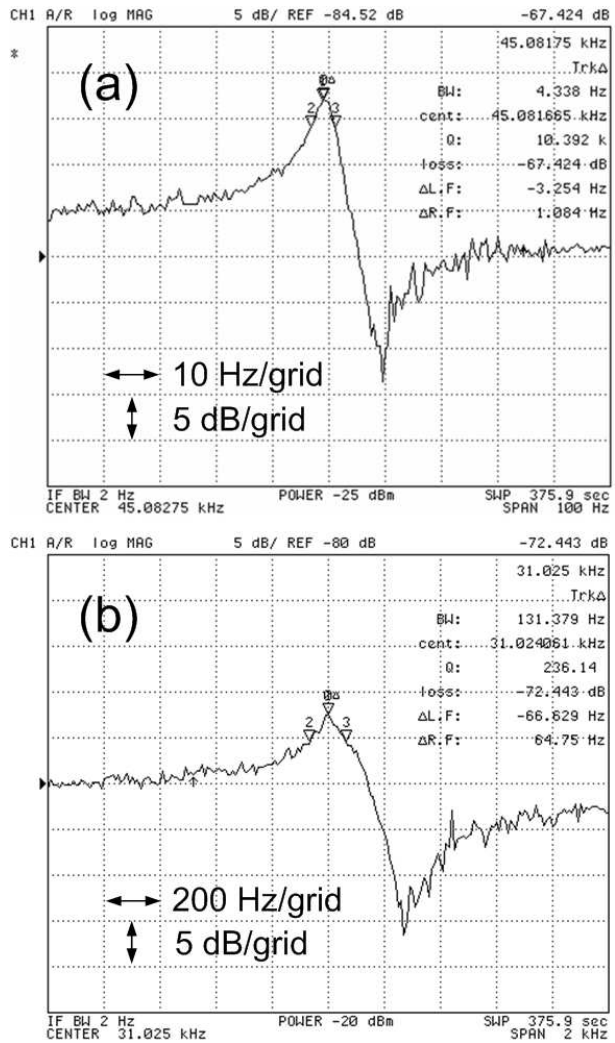

Fig. 4. Typical magnitude plots from a poly-SiC resonator fabricated from the folded-beam device D_{f1} (a) and the device D_{c2} (b) for a straight-beam poly-SiC lateral resonator. The quality factor is around 10,392 at 45,081 Hz for D_{f1} and 236 at 31.025 kHz for D_{c2}.

Figures 4(a) and 4(b) show the magnitude plot for the devices D_{f1} and D_{c1}. The locations of the 3 dB bandwidth for this spectrum are marked with two small inverse triangles, "2" and "3". Note that both of the vertical grids in the magnitude plots represent 5 dB, but the horizontal grids show 10 Hz and 200 Hz, respectively. Owing to the occurrence of the parasitic capacitance, which is mostly due to wire bonding, the antiresonance peak becomes obvious.[23] The findings show that the resonators made from the two folded-beam devices, denoted as D_{f1} and D_{f2}, produced a much higher quality factor reaching about 10,000 [Fig. 4(a)]. This was compared with the

Table 2. Summary of measured resonators.

Device	Resonant frequency (Hz)	Quality factor
D_{f1}	45081	10844
D_{f2}	46812	11962
D_{c1}	29980	679
D_{c2}	31025	236

devices using straight beams with supporting beams of 150 μm, denoted as D_{c1} and D_{c2}, having Q's of about 200–700 [Fig. 4(b)], as presented in Table 2. The results strongly suggest that clamping losses play a significant role in SiC resonators. The Q could not have been acquired for the straight-beam resonator with 100 μm, probably because it was too low compared to the noise floor.

4. Analysis

4.1. *Gas friction*

The gas dissipation of flexural resonators can be considered negligible if the ambient pressure is reduced to a certain level called the critical point.[8,24] Viscous damping is the dominant form of energy dissipation above this pressure, and the gas velocity is zero at the gas–surface interface. However, the gas rarefaction effect is considered at a low pressure with nonzero velocity at the interface, causing gas friction. The gas friction is described as[16,25]

$$Q^{-1}_{\text{gas-friction}} \simeq \frac{pA}{M_e \omega_0 \nu}\,, \tag{4}$$

where p is the gas pressure, A the surface area of the resonator, M_e the effective mass of the resonator, ω_0 the resonant frequency, and ν the thermal velocity of the gas. Figure 5 shows the plot of the normalized quality factor versus the pressure for a poly-SiC folded-beam (device D_{f1}) and a straight-beam resonator (device D_{c1}). Q_b is the quality factor at the lowest pressure in the measurement range, while Q' is the quality factor measured at a particular pressure. The results indicate that the critical point for the straight-beam resonator design used in this study is about 1 Torr, while that for the folded-beam resonator design is about 10 m Torr. The aforementioned findings verify that viscous damping is a more significant component of the total energy dissipation to the straight-beam resonator than that of the folded-beam resonator. The gas dissipations of the resonators measured below the critical point are ideally logarithm decay as shown in Fig. 5. Moreover, the gas friction has little effect on the overall energy dissipation at the critical point of gas damping/friction pressure. In other words, the gas friction has a small ratio of energy losses in these measurements.

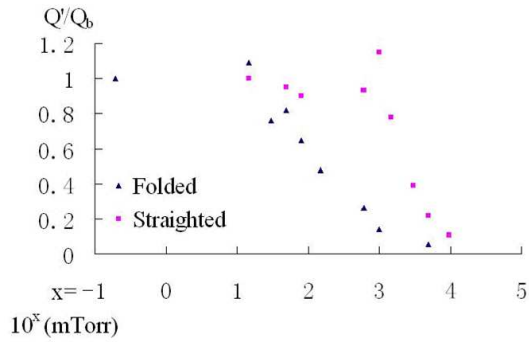

Fig. 5. Normalized quality factor versus pressure for a folded-beam and a straight-beam resonator. Q_b is the quality factor at the lowest pressure in the measurement range, while Q' is the quality factor measured at a particular pressure.

4.2. *Internal material losses and TED*

The material internal loss of a resonator is completely related to the material properties and is largely due to the heat dissipated, i.e. the grain size.[15,16,24,25] A previous report on a single-crystal folded-beam resonator has a Q of about 50,000.[16] In other words, the internal material losses of these polycrystalline SiC resonators make up about 80% of the material losses of single-crystal resonators. However, these material losses are dependent on the fabrication process. The grain size of polycrystalline SiC can affect their material dissipation.

The two types of resonators (D_f and D_c) in this study were manufactured side by side, and the internal loss was expected to have minimal difference. For an oscillating flexural beam resonator, the relaxation rate of the bending beams affects the TED.[26,27] Additionally, the estimated minimal energy dissipation due to TED was calculated using Eqs. (5) and (6)

$$Q_{\mathrm{TED}}^{-1} = \frac{\alpha^2 TE}{\rho C_p} \cdot \frac{F/F_0}{1+(F/F_0)^2} \quad \text{if } F \ll F_0\,, \tag{5}$$

$$F_0 = \frac{\pi\kappa}{2\rho C_p t^2}\,, \tag{6}$$

where C_p is the heat capacity of the structural material, α the thermal expansion coefficient of the structural material, T the spatially mean temperature of the beam, E the elastic modulus of the structural material, F the resonant frequency, F_0 the characteristic damping frequency, κ is the thermal conductivity of the structural material, ρ the mass density of the structural material, and t the beam thickness. Since the devices used in this study were designed to operate at frequencies in tens of kHz, while F_0 was calculated in MHz, the energy loss $\left(Q_{\mathrm{TED}}^{-1}\right)$ was proportional to the resonant frequency with a slope of $\alpha^2 TE/F_0\rho C_p$. Based on theory, the devices operating at these vibrational frequencies would have been expected to exhibit similar and low energy dissipation. Figure 6(a) shows the TED plot by ANSYS

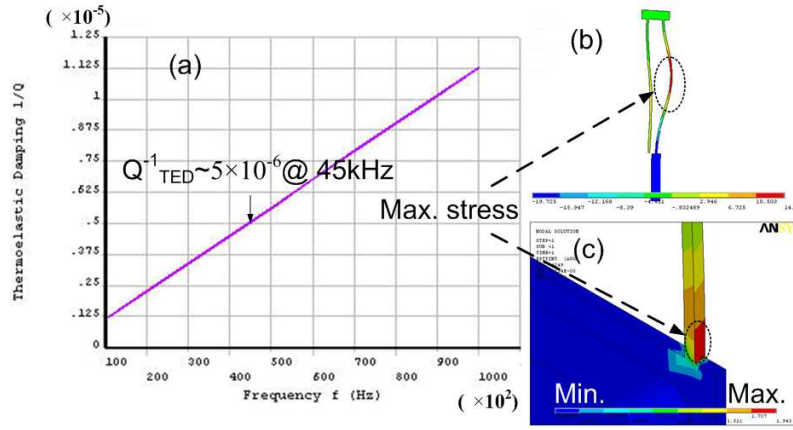

Fig. 6. (Color online). TED plot by ANSYS for a beam of 2 μm thick SiC. The Q_{TED}^{-1} is within the order of 10^{-6} at 45 kHz (a). The plot demonstrates that the highest strain gradient is at about the center of the support beam for a folded-beam resonator (b) and at the joint of the clamping beam of a straight-beam resonator (c), where red signifies the maximum strain gradient, and blue the minimum.

for a beam of 2-μm-thick SiC. The TED between 10 kHz and 110 kHz oscillation frequency was depicted using material type Plane223, which is specified for the 2D thermoelastic model. The curve is nearly linear, due to the low frequency range. The Q_{TED}^{-1} is within the order of 10^{-6} at 45 kHz. TED occurs when the local volume undergoes change, which is due to local stress. Figures 6(b) and 6(c) are representations of the stress distribution, as indicated by a color contour plot. By applying lateral force on the mass proof, the stress plot demonstrates that the highest strain gradient is at about the center of the support beam for a folded-beam resonator [Fig. 6(b)] and at the joint of the clamping beam of a straight-beam resonator [Fig. 6(c)], where red signifies the maximum strain gradient, and blue the minimum [Fig. 6(b)]. Consequently, the results obtained from the calculation showed that the energy dissipation associated with TED is small in the frequency range of the lateral resonators, which is on the order of 10^{-6}, as shown in Table 3. The energy dissipation of type D_f specifically associated with TED was between 4% and 14%, which is indeed small but nonetheless significant. Type D_c has an even lower value of this ratio because it has a much larger Q_{total}^{-1}.

4.3. *Clamping losses*

Clamping loss is a critically important issue for doubly clamped beam resonators. The double clamping design is widely used in MEMS structure, such as RF MEMS switches. In general, the clamping losses for flexural resonators are strongly attributed to the device's design. As such, the two device designs in this study were fabricated side by side on the same chip, thereby ensuring that the microstructure was the same for the two device design types. This was also intended to enable

Table 3. Summary of key material properties and device parameters needed to calculate the contribution of TED to energy dissipation in type D_f.

Material properties	Type D_{f1}
Density (kg/m^3)	3.21×10^3
Heat capacity (J/kg-K)	$5.9 \times 10^2 - 7.0 \times 10^2$ (Ref. 28)
Thermal expansion (1/K)	2.9×10^{-6} (Ref. 29)
Temperature (K)	3.0×10^2
Young's modulus (Pa)	4.0×10^{11} (Ref. 17)
Thermal conductivity (W/m-K)	$8.0 \times 10^1 - 1.8 \times 10^2$ (Ref. 28)
Beam thickness (m)	2.0×10^{-6}
Resonant frequency (Hz) 4.5×10^4	
Q_{TED}^{-1}	$4.4 \times 10^{-6} - 14 \times 10^{-6}$
Q_{total}^{-1}	1.0×10^{-4}
$Q_{\text{TED}}^{-1}/Q_{\text{total}}^{-1}$	$4.0 \times 10^{-2} - 1.4 \times 10^{-1}$

direct comparison. The quality factors for the straight- and folded-beam resonators fabricated from the unmodified LPCVD poly-SiC have significant difference. The data obtained in this study indicate that the clamping loss of the folded-beam resonator can be reduced by more than 10 times compared to that of the straight-beam resonator. Since the damping caused by gas friction is negligible under low pressure, the energy dissipation mechanism of a folded-beam resonator in Eq. (1) is rewritten as follows:

$$Q_{\text{total}}^{-1} \cong \underbrace{(0.04\text{–}0.14)Q_{\text{total}}^{-1}}_{Q_{\text{TED}}^{-1}} + \underbrace{0.8Q_{\text{total}}^{-1}}_{Q_{\text{material}}^{-1}} + Q_{\text{clamping}}^{-1} + \cdots . \tag{7}$$

The above equation estimates the Q_{clamping}^{-1} to be 0.06×10^{-4}–0.16×10^{-4}. Thus, the coefficient β of the folded-beam resonator is between 0.7 and 1.8 using Eq. (2) and the device dimensions in Table 1. However, this coefficient was somewhat too high compared to those used in previous studies,[20,21] although it was a folded-beam resonator. This result may imply that the effective length of type D_f should include part of the proof mass when Eq. (2) is applied to estimate clamping damping. That is to say, the effective beam dimensions should cover the proof mass, and then Eq. (2) should be used to estimate clamping dissipation. Additionally, this value suggests that the proof mass in this design results in a more effective beam width than a beam length. With respect to the straight-beam resonator, the coefficient β may need further study to compare its counterpart made of a single-crystal SiC so as to eliminate the effect of material damping.

5. Conclusion

This study has presented an analysis of the key components that contribute to energy dissipation in 3C-SiC-based MEMS lateral resonators. The data obtained

from the experiments show that TED is small for the frequency range of these devices. The clamping losses are responsible when one is comparing the energy dissipation mechanism of these two types of resonators. The folded-beam design exhibits 10-times-lower losses compared to a straight-beam resonator at the same level of resonant frequency. The coefficient of clamping loss of the folded-beam resonator is calculated to be between 0.7 and 1.8. This suggests that the effective dimension of a folded-beam resonator should be modified due to proof mass. In this study, the proof mass in this design resulted in a more effective beam width than a beam length.

Acknowledgments

The author would like to thank Prof. Christian Zorman for his helpful comments on this paper.

References

1. F. D. Bannon, J. R. Clark and C. T.-C. Nguyen, *IEEE J. Solid-State Circuits* **35**, 512 (2000).
2. J. F. Gong, Z. Y. Xiao and C. H. Chan, *J. Micromech. Microeng.* **17**, 20 (2007).
3. X. M. H. Huang *et al.*, *New J. Phys.* **7**, 1 (2005).
4. R. Leach, Z. Cui and D. Flack, Microsystems technology standardization roadmap project, IST-2001-37682 funded by EU IST program (2001).
5. X. M. H. Huang *et al.*, *Nature* **421**, 496 (2003).
6. J. Yang, T. Ono and M. Esashi, *J. Microelectron. Syst.,* **11**, 775 (2002).
7. P. Mohanty *et al.*, *Phys. Rev. B* **66**, 085416 (2002).
8. F. R. Blom *et al.*, *J. Vac. Sci. Tech. B* **1**, 19 (1992).
9. C. Gui *et al.*, *J. Micromech. Microeng.* **5**, 183 (1995).
10. R. N. Candler *et al.*, Investigation of energy loss mechanisms in micromechanical resonators, in *12th Int. Conf. on Solid State Sensor, Actuator and Microsystem*, Boston, June (2003), pp. 332–335.
11. K. Y. Yasumura *et al.*, *J. Microelectromech. Syst.* **9**, 117 (2000).
12. Y. Wang *et al.*, *J. Phys. Chem. B* **107**, 14270 (2003).
13. T. V. Roszhart, The effect of thermoelastic internal friction on the Q of micromachined silicon resonators, in *Proc. IEEE Solid-State Sensor and Actuator Workshop* (1990), pp. 13–16.
14. R. N. Candler *et al.*, *IEEE J. Microelectrom. Syst.* **15**, 927 (2006).
15. V. T. Srikar and S. D. Senturia, *IEEE J. Microelectrom. Syst.* **11**, 499 (2002).
16. W. T. Chang, M. Mehregany and C. Zorman, Energy dissipation in folded-beam MEMS resonators made from single crystal and polycrystalline 3C-SiC films, in *Proc. of IEEE-NEMS 2007* (2007), pp. 740–744.
17. C. M. Su *et al.*, *J. Appl. Phys.* **77**, 5611 (1995).
18. D. Heinen, H. G. Bohn and W. Schilling, *J. Appl. Phys.* **78**, 893 (1995).
19. W.-T. Hsu, J. R. Clark and C. T.-C. Nguyen, Q-optimized lateral free-free beam micromechanical resonators, in *Proc. 11th Int. Conf. on Solid-State Sensors and Actuators*, Munich, Germany (2001), pp. 1110–1113.
20. Y. Jimbo and K. Itao, *J. Horolog. Inst. Japan* **47**, 1 (1968).

21. X. L. Feng *et al.*, Dissipation in single-crystal 3C-SiC ultra-high frequency nanomechanical resonators, in *Solid-State Sensor, Actuator and Microsystems Workshop* (2006), pp. 86–89.
22. X. A. Fu *et al.*, *Sens. Act. A* **119**, 169 (2005).
23. W.-T. Chang, Modeling of feedthrough capacitance for MEMS folded-beam silicon carbide resonators, in *Electron Devices and Solid-State Circuits* (2007), pp. 298–304.
24. C. J. Welham, J. Greenwood and M. M. Bertioli, *Sens. Act. A* **76**, 298 (1999).
25. T. Veijola and M. Turowski, *J. Microelectron. Syst.* **10**, 263 (2001).
26. T. V. Roszhart, The effect of thermoelastic internal friction on the Q of micromachined silicon resonators, in *Tech. Digest, 4th IEEE Solid-State Sensor and Actuator Workshop* (1990), pp. 16–19.
27. R. Lifshitz and M. L. Roukes, *Phys. Rev. B* **61**, 5600 (2000).
28. A. K. Collins, M. A. Pickering and R. L. Taylor, *IEEE J. Appl. Phys.* **68**, 6510 (1990).
29. A. F. Pojur, B. Yates and B. T. Kelly, *J. Phys. D: Appl. Phys.* **5**, 1321 (1972).